AIAA AVIATION Forum
5-9 June 2017, Denver, Colorado
35th AIAA Applied Aerodynamics Conference

10.2514/6.2017-4367

Surrogate-Based Optimization Applied to Benchmark Aerodynamic Design Problems

Yu Zhang[1] and Zhong-Hua Han[2*],
National Key Laboratory of Science and Technology on Aerodynamic Design and Research, School of Aeronautics, Northwestern Polytechnical University, Xi'an, 710072, P. R. China

Leifur Leifsson[3]
Iowa State University, Ames, Iowa, 50011

The AIAA aerodynamic design optimization discussion group has defined six benchmark aerodynamic design problems for reseachers to present and compare their optimization methods and results. This work applies a surrogate-based optimization (SBO) method based on kriging model and expected improvement (EI) to three benchmark cases, for demonstrating the SBO-type method's capability and applicability of expensive aerodynamic shape optimization. These cases include drag minimization of a NACA0012 airfoil and a NACA0012-based rectangular wing in inviscid flow, and a common research model wing in viscous flow. An adaptive design space technique is used to reduce the computational cost of the optimizations. For the first NACA0012 airfoil case, using CST parameterization method, the SBO can get comparable result with gradient-based method. For the rectangular wing case, with the twist distribution parameterized by B-spline, a lift distribution close to elliptical is obtained. For the optimization of CRM wing using FFD parameterization method, the drag coefficient is reduced by 4 counts at present stage and a practical design is obtained. The results indicates that the results of SBO method is comparable to that of other optimization methods, and has been matured to a stage that can be used to efficiently address expensive engineering design problems.

Nomenclature

Area	=	area of the airfoil
C_l	=	lift coefficient
C_d	=	drag coefficient
C_m	=	moment coefficient
c	=	chord length of the airfoil
Ma	=	Mach number of the flow
Re	=	Reynolds number of the flow

I. Introduction

AN important issue associated with surrogate-based aerodyanmci design optimization[1,2,3,4,5,6,7] is that how to determine the design space. As we can see, the design space of ADO is complex and highly related to the geometric parameterization method[8]. For most of the parameterization methods, the coefficients or design variables

[1] PhD candidate, Department of Fluid Mechanics, Youyi West Road No. 127, P.O. Box754, Student Member AIAA.
[2] Professor, Department of Fluid Mechanics, Youyi West Road No. 127, P.O. Box754, Member AIAA.
[3] Assistant Professor, Department of Aerospace Engineering, Senior Member AIAA.

are coupled with each other. Consequently, different combination of design variables can result in airfoils which are very close to each other. To obtain the optimal result, it seems like the design space should be as large as possible. However, it is more likely to come into a lot of odd airfoils, resulting that the optimization is quite difficult.

To address this issue, we presented a multi-round optimization strategy in our 2016 SciTech Paper[9] and applied it to two benchmark aerodynamic optimization problems[10]: (1) the drag minimization of the NACA 0012 airfoil in transonic inviscid flow; (2) the drag minimization of the RAE 2822 airfoil in transonic viscous flow. The results show that this method is suitable for global optimization and quite good results are found. The results has been compared with that of the gradient-based method[11], which shows that quite good results can be obtained by surrogate-based optimization method. With the class-shape transformation (CST) parameterization method, the impact of dimensionality was also studied in reference 9. However, the efficiency and optimal result of multi-round optimization method is not good enough, especially for the NACA0012 case.

Hence, to further improve the efficiency of surrogate-based optimization and explore better optimal results, we propose an adaptive method for adjusting the design space of a surrogate-based optimization (SBO) and systematically study the influence of mesh size and flow solver on optimal result. Now the method has been employed for three benchmark cases. For the drag minimization of NACA0012 arifoil case, updated results are presented. The results of case 3 and case 4 using the proposed method are also presented.

II. Optimization Methodology

In our 2016 SciTech Paper[9], a surrogate-based multi-round optimization strategy is proposed, to explore the global optimum of airfoil design problems. The essence of this method is that the design space in each round is adjusted on the basis of the optimal airfoil of previous round; meanwhile the optimal airfoil of previous round is taken as one of the initial samples of the next round; in addition, a part of samples of previous round are also taken as initial samples of the next round to speed up the process of the optimization and save the computational cost. The multi-round optimization terminates, when the difference of optimal objectives of two round optimization is less than a threshold.

An adaptive design space technique is developed based on the multi-round optimization method. This method automatically adjusts the design space during the optimization to guide the design to optimum, while all the sample data is used to construct the surrogate models. In this way, for global optimization using SBO, the design space is avoided to be too large to generating odd designs, and compared with the multi-round optimization method, it is more efficient and practical.

For each round optimization, an in-house optimization platform named "SurroOpt"[12,13] is used, shown in Figure 1. After setting the design space, the initial samples are generated by design of experiments (DoE)[14,15]. "SurroOpt" offers functionality of Latin hypercube sampling (LHS)，uniform design (UD) and Monte Carlo design (MC), and we use Latin hypercube sampling (LHS) here. Then the samples are evaluated by CFD analysis. After that, the surrogate models can be constructed both for the objective functions and the constraints. There are different surrogate models such as quadratic response surface model (PRSM), kriging, gradient-enhanced kriging (GEK)[16], Cokriging[17], hierarchical kriging (HK)[18], radial-basis functions (RBFs) available in "SurroOpt". Here kriging model is constructed in this study. Then the kriging models are refined by adding new points selected by specified infill criteria. "SurroOpt" mainly provides five infill sampling criteria[19], such as minimizing surrogate prediction (MSP), and minimizing lower confidence bounding (LCB), maximizing expected improvement (EI), maximizing probability of improvement (PI), and maximizing mean squared error (MSE). In our study, the infill criterion refers to maximizing the constrained expected improvement (EI). This criterion assumes that there is a normal distribution at each site; meanwhile the response and the mean squared error predicted by surrogate model serve as the mean value and the standard deviation. So EI is defined as the mathematical expectation of improvement compared to the optimal solution observed so far. We get the maximum EI position by combining GA with local optimization, such as Hooke and Jeeves pattern search, quasi Newton's methods (BFGS) and sequential quadratic programming (SQP). And the iteration terminated condition is

$$\left\| x^{(i+1)} - x^{(i)} \right\| < \varepsilon_1 \text{ or } N \geq N_{\max} \tag{1}$$

Where N_{max} is the user-specified maximal number of CFD evaluations, and $\varepsilon_1 = 1e-10$. When there is no new sample can be found or the number of samples reaches the maximum, a round of optimization terminates.

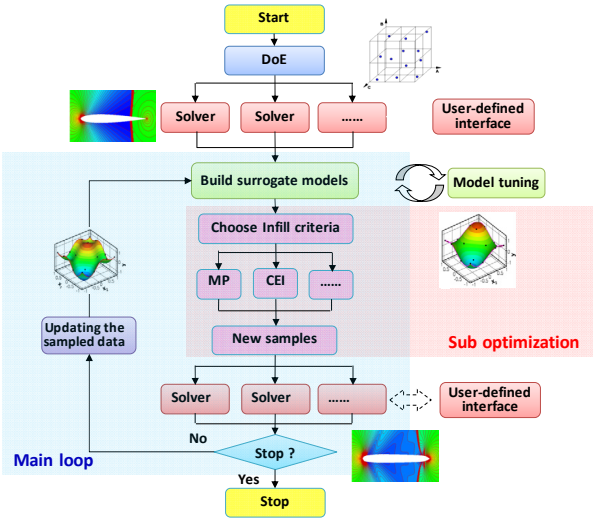

Figure 1. Framework of surrogate-based optimization in SurroOpt

III. Benchmark Case 1: Drag Minimization of the NACA 0012 in Transonic Inviscid Flow

A. Problem Statement

The optimization problem of this work is the drag minimization of a modified NACA0012 airfoil at a freestream Mach number of 0.85 at a zero angle of attack, subject to a full thickness constraint. It can be written as a standard nonlinear programming problem

$$\begin{aligned} &\min \quad C_d \\ &s.t. \quad C_l = 0.0 \\ &\qquad y \geq y_{\text{baseline}} \quad \forall x \in [0,1]. \end{aligned} \tag{2}$$

The modified NACA0012 airfoil with zero thickness trailing edge is defined as

$$y_{baseline} = \pm 0.6\left(0.2969\sqrt{x} - 0.1260x - 0.3516x^2 + 0.2843x^3 - 0.1036x^4\right). \tag{3}$$

B. Parameterization method

The CST method[33] is adopted to parameterize the airfoils. Its mathematical expression is

$$\begin{aligned} &y(x) = C_{N2}^{N1}(x)\cdot S(x) + x\cdot \mathrm{y_{TE}}, \qquad \mathrm{y_{TE}} = \Delta \mathrm{y_{TE}}/c \\ &C_{N2}^{N1}(x) = x^{N_1}(1-\mathrm{x})^{N_2} \\ &S(x) = \sum_{i=0}^{p} A_i B_{i,p}(x), \mathrm{S(0)} = \sqrt{2R_{\mathrm{LE}}/C}, \mathrm{S(1)} = \tan\beta + \Delta y_{\mathrm{TE}}/C \end{aligned} \tag{4}$$

Where the term $C_{N2}^{N1}(x)$ represents the "class function" which is used to define general classes of geometries and the term $S(x)$ is the "shape function" which is used to define specific shapes within the geometric class. Especially $S(0)$ is directly related to the normalized airfoil leading-edge nose radius R_{LE} and $S(1)$ is directly related to the airfoil boat-tail angle β and normalized trailing-edge thickness Δy_{TE}. The shape function is represented by summing up of the Bernstein polynomials, so their coefficients, A_i, serve as the design variables of our airfoil design problem.

First, we set the class function exponents $N_1 = 0.5$ and $N_2 = 1.0$ to define a round nose and pointed-aft-end-typed airfoil, and fix the parameters during the optimization. Second, we adopt the two parameters as design variables as well, to see its influence on the optimization.

C. Review of results of Multi-round SBO Method

The O-type mesh for inviscid flow simulation are generated by solving elliptic equations with very good uniformity and orthogonality. An in-house CFD code called "PMNS2D"[20,21] is used as the flow solver. The class-shape transformation (CST) method[8] is adopted to parameterize the airfoils and the result of optimization with 17 variables is depicted here. Grid study for baseline airfoil is conducted and the typical grids used for optimization have 320 points in the stream-wise direction and 160 points in the direction normal to the airfoil surface.

For the multi-round optimization, it is conducted until all of the design variables of optimal airfoil are within the design space in the fourth round. To guarantee that the optimization is full converged, an addition local optimization is conducted further, which is the fifth-round optimization. Figure 2 shows the process of the drag coefficient reduction in the multi-round optimization. As we can see, the decrease of drag coefficient is slowing down which means the optimization converges. **An optimized airfoil with the drag coefficient of 73.08 cts is obtained using 932 CFD evaluations.** The force coefficient of the optimal airfoil in each round is shown in Table 1. Figure 3 shows the comparison of Mach number contours for baseline and final optimal airfoils. It is clearly shown that the strongly shock wave on the NACA 0012 airfoil surface is broken into an attached shock wave and a detached shock wave. Since the attached shock wave is much weaker, the shock wave drag is greatly reduced. The thorough study of the multi-round optimization, the impact of the dimensionality and grid for baseline and optimal airfoil were presented in the 2016 SciTech Paper[9].

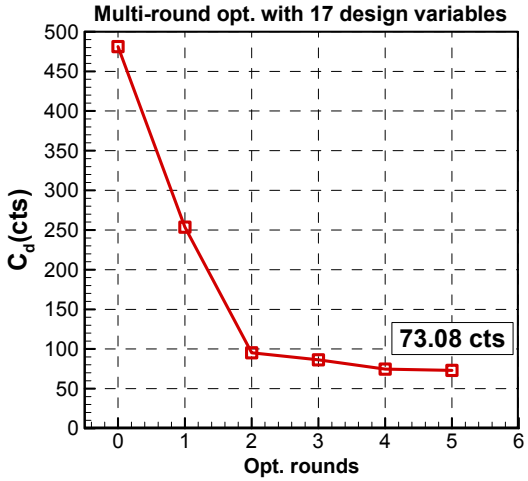

Figure 2. Convergent history of drag coefficient in multi-round optimization for NACA 0012 airfoil test case (Ma=0.85, AoA=0°)

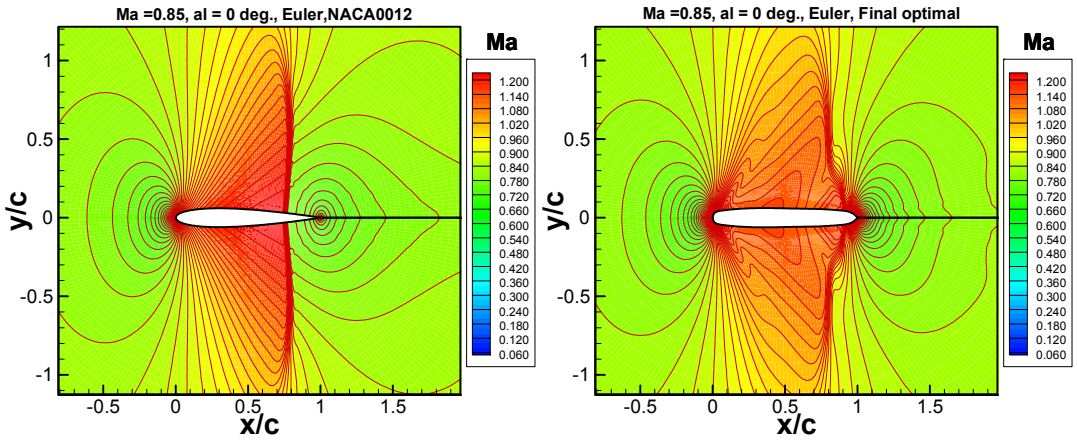

Figure 3. Comparison of Mach number contours of baseline and final optimal airfoils in multi-round optimization for NACA 0012 airfoil test case (Ma=0.85, AoA=0°)

Table 1. Force coefficients of optimal airfoil in each round for NACA 0012 airfoil test case (Ma=0.85, AoA=0°)

Variable	Baseline	1st round Opt.	2nd round Opt.	3rd round Opt.	4th round Opt.	5th round Opt.
C_l (cts)	0.0	0.0	0.0	0.0	0.0	0.0
C_d (cts)	481.28	253.52	95.24	86.42	74.70	73.08
N_CFD	/	167	184	206	275	100

D. Results of SBO with Adaptive adjusted Design Space

Then, we adopt the adaptive design space method for the NACA 0012 case. In the optimization process, all of the sample data is adopted to construct the surrogate models, while the new design is choosed by EI in a specific design space determined by the observed optimum. Figure 4 shows the convergent history of this method, and it is compared with that of multi-round optimization. We can see that it can greatly improved the optimization efficiency. Table 2 shows the value of objective, when the same number of CFD evaluations is employed. Table 3 shows the least number of CFD calls required to achieve a certain value of objective for the two methods. **We can clearly see that the adaptive design space method can improve the optimization efficiency by two times. If we take that the C_d lower than 100 cts as a acceptable standard, for the adaptive design space method, only 167 CFD calls is needed to meet the requirement, which is a quite acceptable computational cost.**

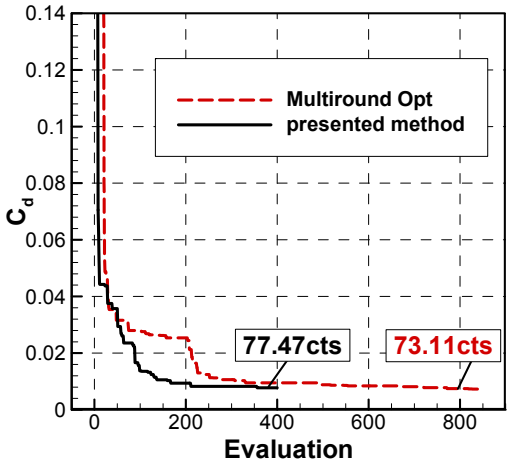

Figure 4 Comparison of convergent history of single-round SBO with adaptive adjusted design space and multi-round optimization method (Ma=0.85, AoA=0°)

Table 2. Comparison of force coefficients of optimal airfoils with the same number of CFD calls (Ma=0.85, AoA=0°)

		Multi-round optimization	Presented method
C_d	when 100 CFD calls	279.83 cts	137.65 cts
	when 200 CFD calls	253.52 cts	93.75 cts
	when 350 CFD calls	95.24 cts	77.47 cts
	when 720 CFD calls	77.82 cts	/
	when 850 CFD calls	73.11 cts	/

*The number of CFD calls is an approximate number.

Table 3. Comparison of CFD calls of optimal airfoils with the same value of objective (Ma=0.85, AoA=0°)

		Multi-round optimization	Presented method
Least No. of CFD calls	when $C_d \leqslant 200$ cts	213 (185.68cts)	89 (166.15cts)
	when $C_d \leqslant 100$ cts	330 (98.05cts)	167 (93.75cts)
	when $C_d \leqslant 80$ cts	721 (77.82cts)	356 (77.47cts)

E. Results of SBO with Adaptive and Expanded Design Space

Besides that, as the CST method[8] is adopted to parameterize the airfoils, we also studied the influence of the parameter in CST on the optimization efficiency. For the "multi-round strategy", as usual, we set the exponents in class function $N_1 = 0.5$ and $N_2 = 1.0$ to define the round nose and pointed-aft-end-typed airfoil. However, we can see that the shape of optimal airfoil is very different with that of the baseline, NACA0012, and it can be considered as a round-nose and aft-end-typed airfoil. In this way, both the exponents N_1, N_2 in class function should be 0.5. As we do not expect it in the first, we take N_1, N_2 as the design variables to obtain a more complete design space, and this method is called the SBO with expanded design space.

Figure 5 shows the convergent history of SBO with expanded design space, and it is compared with that of SBO with adaptive design space only. Note that for the SBO with expanded design space, the adaptive design space method is also used. We can see that the optimization efficiency is improved remarkablely. Table 4 shows the value of objective, when the same number of CFD evaluations is employed. Table 5 shows the least number of CFD calls required to achieve a certain value of objective for the two methods. Because we take the exponents in class function of CST as the design variables, a more complete design space is obtained, resulting that the drag coefficient is reduced fast. **Only 31 CFD evaluations are needed to obtain an airfoil with drag coefficient around 100 cts. And actually, the exponents in class function for the new optimized airfoil are 0.578 and 0.443, which just confirm our idea.**

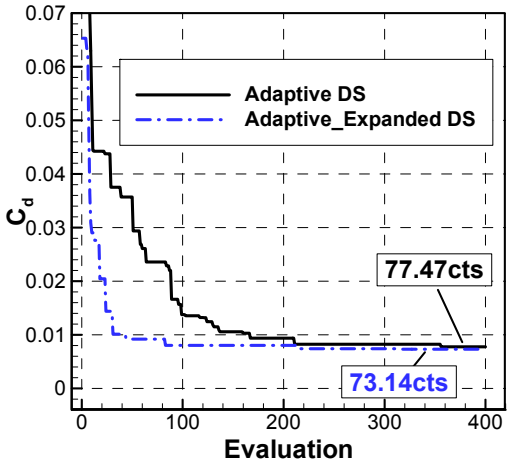

Figure 5 Comparison of convergent history of SBO taking the exponents in class function of CST as design variables or not (Ma=0.85, AoA=0°)

Table 4. Comparison of force coefficients of optimal airfoils with the same number of CFD calls (Ma=0.85, AoA=0°)

		adaptive design space	adaptive and expanded design space
C_d	when 100 CFD calls	137.65 cts	80.44 cts
	when 200 CFD calls	93.75 cts	73.96 cts
	when 350 CFD calls	77.47 cts	73.14 cts

*The number of CFD calls is an approximate number.

Table 5. Comparison of CFD calls of optimal airfoils with the same value of objective (Ma=0.85, AoA=0°)

		adaptive design space	adaptive and expanded design space	
Least No. of CFD calls	when $C_d \leqslant$ 200 cts	89 (166.15cts)	24(143.96cts)	18(204.40cts)
	when $C_d \leqslant$100 cts	167 (93.75cts)	44(91.95cts)	31(101.20cts)
	when $C_d \leqslant$80 cts	356 (77.47cts)	83(80.44cts)	83(80.44cts)

F. Further optimization with finer grid

We have conducted the grid study for NACA0012 airfoil in our 2016 SciTech Paper[9], using an in-house mesh generator by solving elliptic equations. Table 6 shows the grid study with respect to grid size for the initial airfoil NACA 0012. And we can see that the difference in drag coefficients is converging within 0.1 counts gradually with the increase of the number of cells. In view of the computational cost, the grid with 51200 cells (the fourth grid) is taken as the computational grid during the optimization. However, the force coefficients of an airfoil are somehow different, when using the grid with different resolution. And the difference can change for different airfoil.

Table 6. Grid convergence study for the NACA0012 w.r.t. grid size (Ma=0.85, AoA=0°)

Grid size	C_l (cts)	C_d (cts)
128 × 64	0.0	462.70
192 × 96	0.0	478.92
256 × 128	0.0	480.20
320 × 160	**0.0**	**481.28**
384 × 192	0.0	482.32
448 × 224	0.0	482.85
512 × 256	**0.0**	**483.13**
576 × 288	**0.0**	**483.21**

So we further conduct a round of optimization based on the fine grid, which has 131072 cells (the seventh grid), and take the optimal aifoil as the baseline. Figure 6 shows the convergent history, and we can see that the drag coefficient of optimized airfoil is further reduced, and an airfoil with 62.95 cts is obtained. The pressure coefficient distribution of the final optimal airfoil is compared with the airfoil optimized using coarse grid, which is also evaluated by fine grid (that's why the drag coefficient changes from 73.14 cts to 68.39 cts), as shown in Figure 7. The pressure coefficient distributions are extremely similar, and the final design seems to have a little weaker shock wave at the trailing adge of the airfoil.

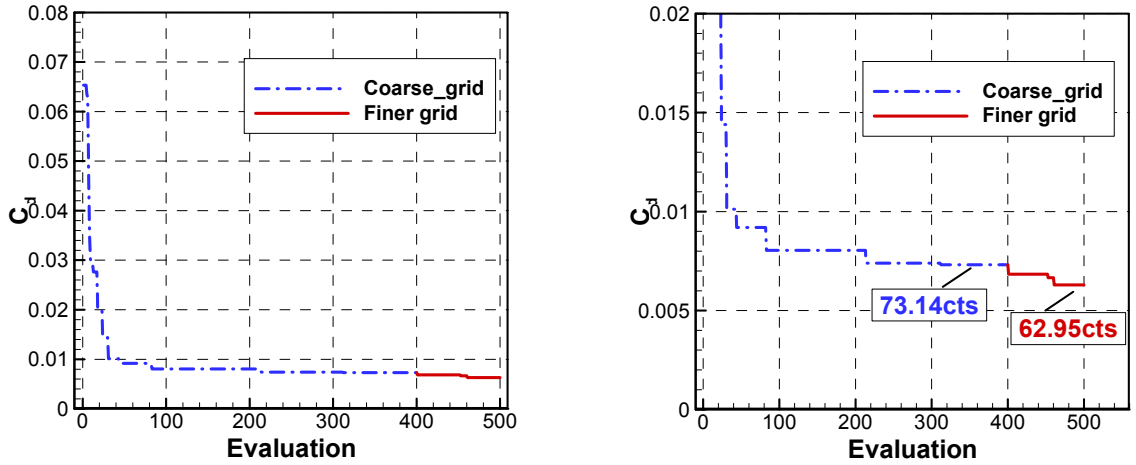

(a) convergent history of C_d (b) zoom-in view

Figure 6 Result of the further optimization based on observed optimal airfoil with fine grid (Ma=0.85, AoA=0°)

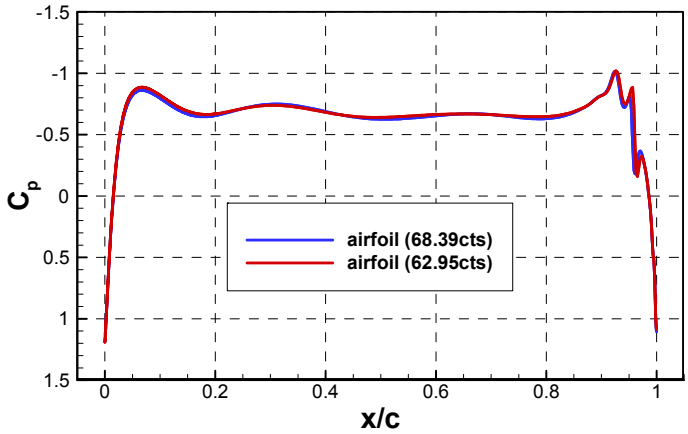

Figure 7 Comparison of pressure coefficient distributions of the airfoils optimized by different grid resolution (Ma=0.85, AoA=0°)

G. Influence of using different Flow solver

As all the optimizations perform on our in-house code PMNS2D, we would like to study the influence of flow solve on the optimal result. So, the optimal airfoil is evalulated by SU2, and the results are compared in Table 7. Here, both the flow solvers employ the grids in same size, which is 512 points in the stream-wise direction and 256 points in the direction normal to the airfoil surface. Figure 8 shows the comparison of pressure coefficient distributions of the final optimal airfoil. **We can see that the pressure coefficient distributions only have very small difference, while the drag coefficients have the difference of 8 cts.**

Table 7. Drag coefficient of optimal airfoil evaluated by PMNS2D and SU2 (Ma=0.85, AoA=0°)

	PMNS2D	SU2
C_d (cts)	**62.95**	**55.10**

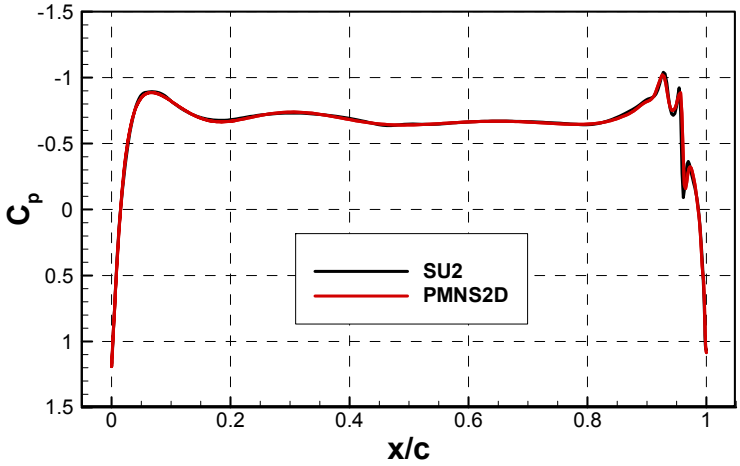

Figure 8 Comparison of pressure coefficient distributions evaluated by SU2 and PMNS2D (Ma=0.85, AoA=0°)

H. SBO based on SU2

Up to now, we can see that, the flow solver have great influence on the optimal results and the drag coefficient evaluated by SU2 is smaller than that of our in-house code PMNS2D. Therefore, for comparison purposes, we plan to perform the optimization using the SU2 solver and four different algorithms: the internal gradient-based search algorithms in SU2, gradient-based search using pyOpt, surrogate-based search with approximation-based models[3], and surrogate-based search using multi-fidelity models and manifold mapping[10]. The details of the approaches will be given in the full paper.

IV. Benchmark Case 3: Twist Optimization of a Rectangular Wing with NACA0012 Sections

A. Problem Statement

This case is to optimize the twist distribution of a rectangular wing to minimize the induced drag at a freestream Mach number of 0.5 at a fixed lift of 0.375. The optimization problem is formulated as:

$$\begin{aligned} &\min \quad C_D(\gamma) \\ &s.t. \quad C_L = 0.375 \\ &\left.\frac{d\gamma}{dy}\right|_{y=3c} \geq -10°/c \end{aligned} \tag{5}$$

Here, γ is the twist distribution of the wing, which is measured relative to the root, as the wing is required to be twisted about the trailing edge. And the twist at the wing tip should be larger than -10 degree. The sectional shape and wing planform are both fixed. The aim of this case is to recover a elliptical lift distribution in inviscid flow.

B. Parameterization method

The geometry of the baseline wing is shown in Figure 9. The baseline is untwisted, unswept, and has zero dihedral, with the sectional shape of a modified NACA0012 airfoil, which is the same as case 1. And the tip of the wing is a surface of revolution based on this airfoil. In our work, the wing tip is pinched for simplicity during the optimization, as the reference 24 indicates that the optimal planform shape depends subtly on the wing-tip shape.

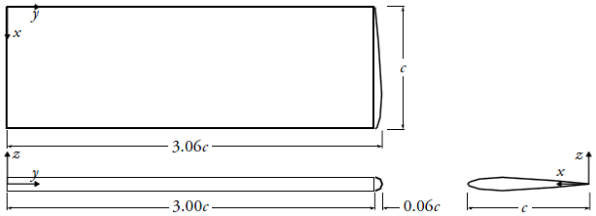

Figure 9 Initial semi-span geometry for case 3

B-spline method is used to parameterize the twist distribution. Four control points distributed uniformly along the wing span are adopted. The control point at the root is fixed and the vertical movement of other three points are permitted, therefore, there are 3 design variables in total. The lower and upper boundry of the design variables are set as $[-6,-6,-6] \sim [6,6,6]$. The angle of attack is not taken as a design variables explicitly, as it is adjusted automatically to make the C_L equal 0.375 during a CFD analysis.

C. Mesh and flow solver

The flow analyses are performed with an in-house code called PMNS3D. The Euler equations are solved by using the cell-centered finite volume method. The second-order Jameson central scheme is used as the spatial discretization scheme, and Runge-Kutta is used for time integration. Implicit residual smoothing, local-time stepping and multigrid techniques are used to accerate the solution converge to the steady state.

Figure 10 shows the C-H type grid used in this paper, which are generated automatically by our in-house code, with the grid distribution of 200 (chord-wise direction) $\times$ 64 (normal direction) $\times$ 80 (span direction). The grid point were clustered at the trailing and leading edge, and the root and tip of the wing. The far field distance is set as 40 chord lengths. The flow simulation is terminated after the density residual has dropped 5.5 orders in magnitude with the lift coefficient fixed at 0.375. The convergence histories of force coefficient and residual are shown in Figure 11. A typical evaluation time of the inviscid CFD simulation is around 2 hours on PC with single precessors.

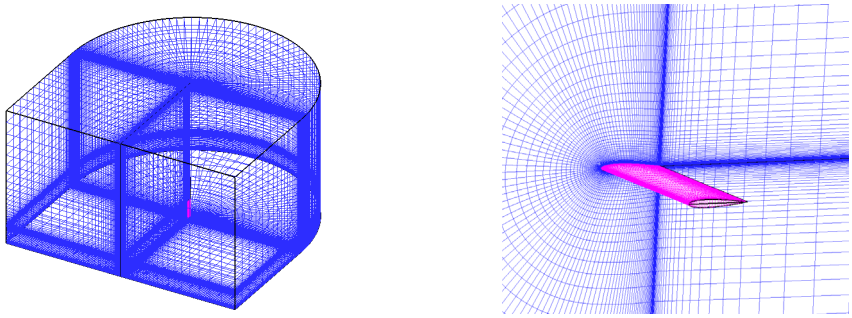

Figure 10 Sketch of C-H mesh for for case 3

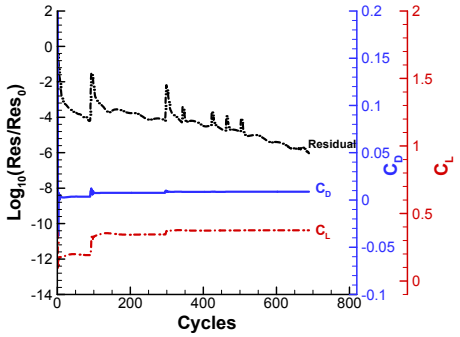

Figure 11 Convergence histories of invisicid simulation for case 3 (Ma=0.85, C_L=0.375)

D. Result

The optimization is conducted using the SBO method (Section II). Ten sample points are evaluated by invisid simulation and used to construct the initial kriging model. Then 14 sample points are added using EI criterion, until the optimum design is obtained. The convergence histories of the objective function versus the number of evaluations, are shown in Figure 12 (left). Figure 12 (right) shows the sectional lift distribution along with the span of the baseline and optimized wing, compared with the elliptical lift distribution, which shows that the optimized one has a sectional lift distribution close to the elliptical one. The lift coefficient, drag coefficient and span efficiency factor e of the baseline and optimized design are shown in Table 8. The span efficiency is given by the formula 6. As we can see, the drag coefficient is reduced from 86.88 to 84.90 counts, and the span efficiency factor grows from 0.8587 to 0.8787. Table 9 shows the twist and sectional lift coeffcient distribution along the span of the baseline and optimized wing respectively, which also shows that the sectional lift distribution is close to elliptical distribution in magnitude.

$$e = \frac{C_L^2}{\pi \Lambda C_D} \tag{6}$$

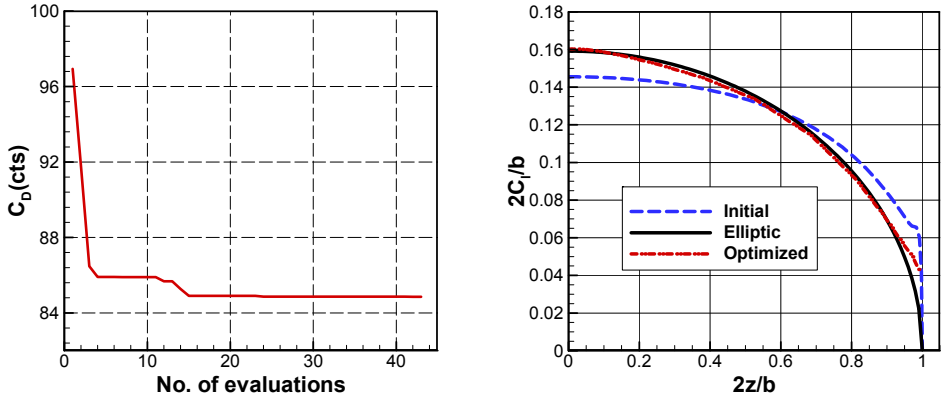

Figure 12 Optimization convergence histories of objective function (left); Sectional lift distribution of baseline, optimized design and elliptical lift distribution (Ma=0.85, C_L=0.375)

Table 8. Comparison of force coefficient of the baseline and optimized wing (Ma=0.85, C_L=0.375)

	α	C_L(cts)	C_D(cts)	e
Baseline	4.126	37.5	86.88	0.8587
Optimized	5.2	37.5	84.85	0.8787

Table 9. Comparison of twist and sectional force coefficient of the baseline and optimized wing (Ma=0.85, C_L=0.375)

	η	0.0	0.2	0.4	0.6	0.8	0.9	0.95	1.0
γ	Baseline	0.0	0.0	0.0	0.0	0.0	0.0	0.0	0.0
	Optimized	0.0000	-0.2704	-0.3561	-0.6044	-1.2517	-1.9598	-2.3345	-2.7971
$2C_L/b$	Baseline	0.1455	0.1438	0.1383	0.1266	0.1027	0.0821	0.0706	0.0423
	Optimized	0.1602	0.1546	0.1434	0.1254	0.09135	0.06921	0.05390	0.0241
	Elliptical	0.1592	0.1559	0.1459	0.1273	0.0955	0.0694	0.0497	0.0

V. Benchmark Case 4.1: Single-Point Optimization of CRM Wing

A. Problem Statement

This objective of this case is to minimize the drag coefficient of the Common Research Model (CRM) wing, which was subject of the Fifth Drag Prediction Workshop. This case is more complex, since both the wing twist and sectional shapes are designable. The optimization problem can be expressed as

$$\begin{aligned} \min \quad & C_D \\ s.t. \quad & C_L = 0.5 \\ & C_M \geq -0.17 \\ & t \geq 0.25 t_0 \\ & V \geq V_0 \\ & \Delta z_{TE} = 0 \\ & \Delta z_{LE,upper,root} = -\Delta z_{LE,lower,root} \end{aligned} \tag{7}$$

The initial geometry is given by the ADODG, and it is scaled by the mean aerodyanmic chord. The aerodynamic constraints include that the lift coefficient is constrained to 0.5, and the pitching-moment coefficient should greater than -0.17, which is taken about the point (1.2077,0,0.007669) with the origin at the leading edge of the wing root. For the geometric constraints, the volume must not be less than the baseline, and the thickness should be greater than or equal to 25% of the initial thickness at all locations. In addition, sectional shape changes are permitted in the vertical direction only. The trailing edge of the wing is fixed, while the leading edge is free, except for the root section, both the leading and trailing adges are fixed. In this way, the wing planform shape is fixed, and the reference area is 3.407014.

B. Parameterization method

A free-form deformation (FFD) method based on bernsterin polynomials is used to parameterize the wing geometry. Figure 13 shows the FFD volume, which covers the whole CRM wing. The change of geometry is performed on the outside control volume and the design variables are the z-coordinates of the FFD control points. There are 4 spanwise design sections, and each is controlled by 6 chordwise FFD control points on the upper and lower, respectively. To satisfy the geometry constraints, the control points at the trailing edge of the wing are fixed. Especially, for the two control points at the leading edge of the root, they are forced to have the same change in magnitude simultaneously in opposite direction due to the geometry constrait. In this way, there are 39 design variables in total.

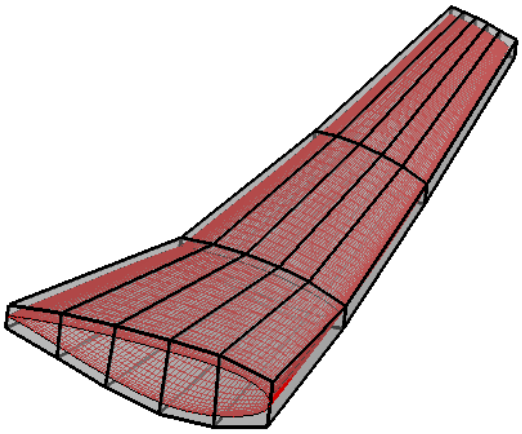

Figure 13 Geometry of the baseline and the initial control frame of FFD for CRM wing

C. Mesh and flow solver

The viscous flow simualtion is also performed with the PMNS3D. The NS equations are solved by using the cell-centered finite volume method. The second-order Jameson central scheme is used as the spatial discretization scheme, and the Spalart-Allmaras one-equation turbulence model is used for turbulence closure. Implicit LU-SGS is used for time integration. Variable-coefficient implicit residual smoothing, local-time stepping and multigrid techniques are used to accerate the solution converge to the steady state.

The mesh (Figure 14) used in this case is generated in ICEM CFD, and has 17 blocks in H-H type. The total number of mesh cells is 778238. The far field distance is set as 70 chord lengths. The flow simulation is terminated after the density residual has dropped 6.0 orders in magnitude. The convergence histories of force coefficient and residual are shown in Figure 15. A typical evaluation time of the inviscid CFD simulation is around 1 hours on PC with single precessor.

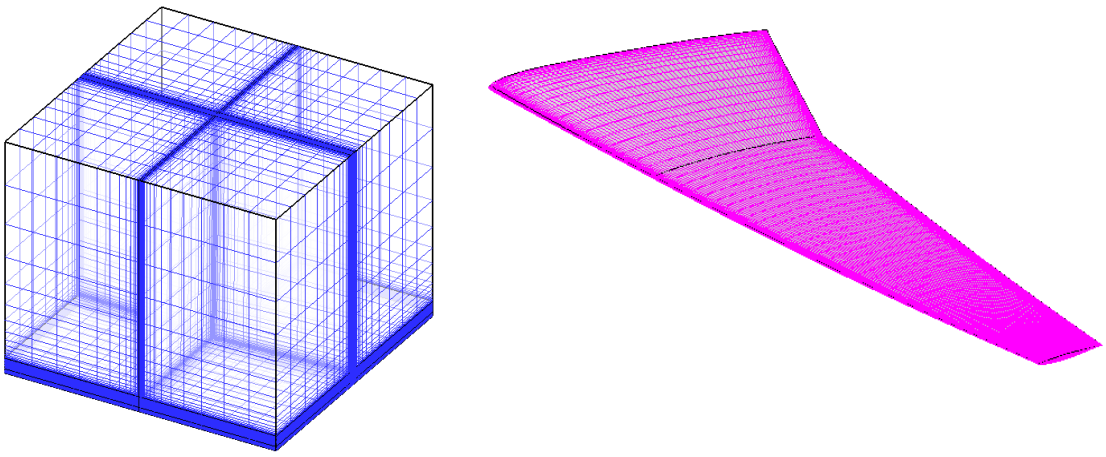

Figure 14 Sketch of H-H mesh for CRM wing

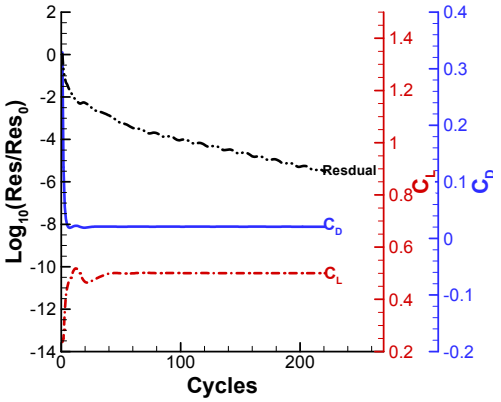

Figure 15 Convergence histories of force coefficient and residual for CRM wing (Ma=0.85, Re=500×10^6, C_L=0.5)

D. Result

The convergence history of the objective function is shown in Figure 16, and the optimization result compared with the baseline are presented in Table 10. The drag coeffcient is reduced from 207.56 to 203.62 counts. For the optimized wing, the lift, moment coefficient and volume constraints are satisfied strictly. The surface pressure contour and sectional pressure cofficient distributions and sectional shapes are shown in Figure 17. For the surface pressure contour, the baseline is shown on the left, and the optimized wing is shown on the right. For the sectional shapes and pressure coefficient distributions, those of the baseline are shown in blue, while they are in red for the optimized wing. The shock wave drag is reduced obviously at the root section and the next section. However, the drag at other sections are not weakened, and the shape of the wing changes a little without a distinct change in thinkness.

According to result, we have obtained a quite good design in current design space, although there is still strong shock wave existing. To get a better design with smaller drag, we should add the control surface of FFD volume, and increase the number of chordwise control point. Also, the SBO method is a global optimization method, which relys on the accuracy of the surrogate model. However, it is hard to construct a global surrogate model with sufficient accuracy for a high-dimensional complex optimization case, and we should further study how to adjust the design space during the optimization for SBO method.

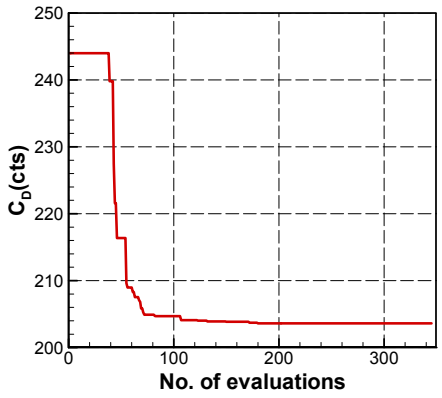

Figure 16 Optimization convergence histories of objective function for CRM wing case (Ma=0.85, Re=500×10^6, C_L=0.5)

Table 10. Optimization results for CRM wing case (Ma=0.85, Re=500×10^6, C_L=0.5)

	C_L	C_D	C_M	V
Baseline	0.500	0.020756	-0.1845	0.2617178
Optimized	0.500	0.020362	-0.1700	0.2617185

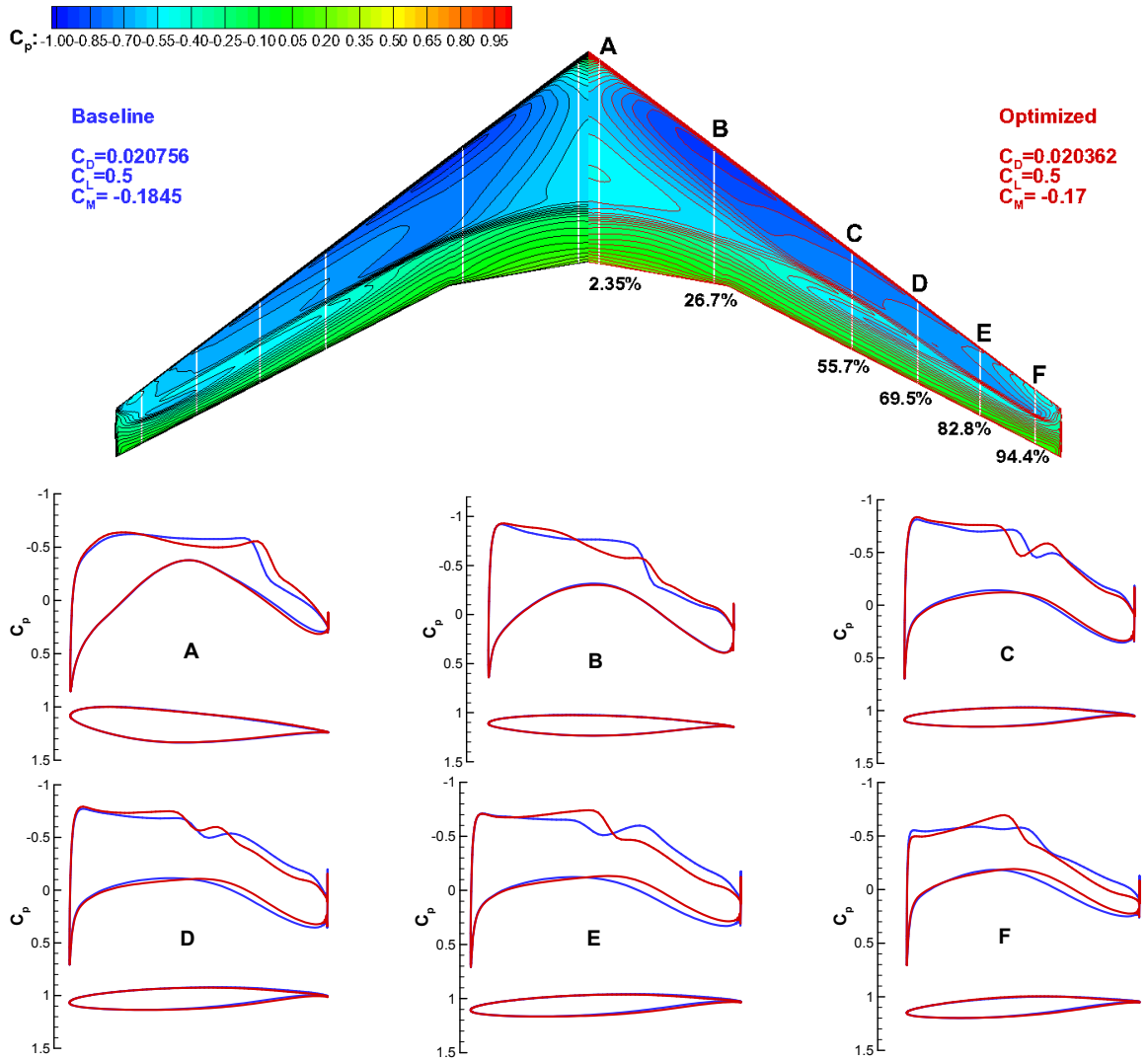

Figure 17 Comparison of surface pressure contour and sectional pressure cofficient distributions and sectional shapes between the baseline and optimized wing (Ma=0.85, Re=500×106, CL=0.5)

VI. Conclusion

In this work, a surrogate-based optimization method is used to find the global optimal solutions of three aerodynamic optimization benchmark problems.

The result of NACA0012 case is updated by using this method, and compared with that of multi-round optimization method. The results show that the adaptive design space method can greatly improve the efficiency of surrogate-based optimization. On the other hand, by taking the class-function exponents of CST method as the design variables, the optimization efficiency is further improved. On the other hand, as the computational mesh have signifcant influence on the optimal result, we conduct a further optimization based on the observed optimal airfoil. We also studied the optimum with another flow solver, SU2, and a smaller drag coefficient is obtained. The results show that the SBO method can get comparable result with the gradient-based method.

For the rectangular wing optimization case, a lift distribution close to elliptical distribution is obtained using the SBO method. After the initial sample points are evaluated to construct the initial surrogate model, only 14 sample points are needed to obtain the optimum, which validates the high efficiency of the proposed method.

For the single-point optimization of CRM wing, the drag coeffcinet is reduced by 4 counts. Although the global optimum for the defined problem has not been found, a practical design is obtained, which shows the potential of SBO method for expensive engineering design problems.

Acknowledgments

This research was supported by the National Natural Science Foundation of China (NSFC) under grant No. 11272265 and by "the Fundamental Research Funds for the Central Universities".

The author would like to thank Dr. Shao-Qiang Han for providing the result of optimal airfoil evaluated by SU2.

References

[1] Queipo, N. V., Haftka, R. T., Shyy, W., Goel, T., Vaidyanathan, R. and Tucher, P. K., "Surrogate-based Analysis and Optimization," *Progress in Aerospace Sciences*, Vol.41, 2005, pp. 1, 28.

[2] Simpson, T. W., Toropov, V., Balabanov, V. and Viana, F. A. C., "Design and Analysis of Computer Experiments in Multidisciplinary Design Optimization: a Review of How We Have Come-or not," AIAA-2008-5802, 2008.

[3] Forrester, A. I. J., Keane, A. J., "Recent advances in surrogate-based optimization," *Progress in Aerospace Sciences*, Vol. 45, 2009, pp. 50-79.

[4] Keane, A. J., Nair, P. B., "Computational Approaches for Aerospace Design: The Pursuit of Excellence," John Wiley & Sons, Ltd, Chichester, 2005.

[5] Koziel, S., Leifsson, L. and Yang, X. S. "Surrogate-based optimization," In S. Koziel, X.S. Yang, Q.J. Zhang (Eds.) *Simulation-Driven Design Optimization and Modeling for Microwave Engineering,* Imperial College Press, London, UK, 2013.

[6] Leifsson, L., Koziel, S., Tesfahunegn, Y.A., "Multiobjective Aerodynamic Optimization by Variable-Fidelity Models and Response Surface Surrogates," *AIAA Journal*, Vol. 54, No. 2, 2016, pp. 531-541.

[7] Leifsson, L., and Koziel, S. "Aerodynamic Shape Optimization by Variable-Fidelity Computational Fluid Dynamics Models: A Review of Recent Progress," *Journal of Computational Science*, Vol. 10, September 2015, pp. 45-54

[8] Kulfan, B. M., "Universal Parametric Geometry Representation Method," *Journal of Aircraft*, Vol. 45, No. 1, 2008, pp. 142-158.

[9] Zhang, Y., Han, Z.-H., Shi, L.-X. and Song, W.-P., "Multi-round Surrogate-based Optimization for Benchmark Aerodynamic Design Problems," AIAA-2016-1545, Jan. 2016.

[10] Ren, J., Thelen, A., Amrit, A., Du, X.-S., Leifsson, L., Tesfahunegn, Y.A. and Koziel, S., "Application of Multi-fidelity Optimization Techniques to Benchmark Aerodynamic Design Problems," AIAA paper 2016-1542, 2016.

[11] Tesfahunegn, Y. A., Koziel, S., Gramanzini, J. R., Hosder, S., Han, Z. H. and Leifur L. "Application of Direct and Surrogate-Based Optimization to Two-Dimensional Benchmark Aerodynamic Problems: A Comparative Study," AIAA paper 2015-0265, 2015.

[12] Han, Z.-H., "SURROOPT: A generic surrogate-based optimization code for aerodynamic and multidisciplinary design," 30th congress of the international council of the aeronautical sciences, Korea, 2016.

[13] Han, Z.-H., "Kriging Surrogate Model and Its Application to Design Optimization: A Review of Recent Progress," *Chinese Journal of Aeronautics*, http://www.cnki.net/kcms/detail/11.1929.V. 201603291455.004.html， 2016.

[14] Simpson, T. W., Toropov, V., Balabanov, V. and Viana, F.A.C., "Design and analysis of computer experiments in multidisciplinary design optimization: a review of how far we have come - or not," AIAA paper 2008-5802, 2008.

[15] Giunta, A. A., Wojtkiewicz, S. F. and Eldred, M. S., "Overview of modern design of experiments methods for computational simulations," AIAA paper 2003-649, 2003.

[16] Han, Z.-H., "Improving Adjoint-based Aerodynamic Optimization via Gradient- Enhanced Kriging," AIAA-2012-0670, 2012.

[17] Han, Z. -H., Zimmermann, R., and Goertz, S., "an Alternative Cokriging Model for Variable-Fidelity Surrogate Modeling," *AIAA Journal*, Vol. 50, No. 5, 2012, pp. 1205-1210.

[18] Han, Z. -H., and Goertz, S., "Hierarchical Kriging Model for Variable-Fidelity Surrogate Modeling," *AIAA Journal*, 2012, Vol. 50, No. 5, 2012, pp. 1285-1296.

[19] Liu, J., Han, Z.-H., and Song, W.-P., "Comparison of Infill Sampling Criteria in Kriging-based Aerodynamic Optimization," 28th international congress of the aeronautical sciences, Brisbane, Australia, 2012.

[20] Xie, F., Song, W. P. and Han, Z. H., "Numerical Study of High-Resolution Scheme Based on Preconditioning Method," *Journal of Aircraft*, Vol. 46, No. 2, 2008, pp. 520-525.

[21] Han, Z. H., He, F., Song, W. P. and Qiao, Z. D., "A Preconditioned Multigrid Method for Efficient Simulation of Three-dimensional Compressible and Incompressible Flows," *Chinese Journal of Aeronautics*, Vol. 20, No. 4, 2007, pp. 289–296.

[22] Liu, J., Song, W. -P., Han, Z. -H., and Zhang, Y., "Efficient Aerodynamic Shape Optimization of Transonic Wings Using a Parallel Infilling Strategy and Surrogate Models," *Structural and Multidisciplinary Optimization* (2016). http://link.springer.com/article/10.1007/s00158-016-1546-7. doi:10.1007/s00158-016-1546-7.

[23] Kulfan, B. M., "Universal Parametric Geometry Representation Method," Journal of Aircraft, Vol. 45, No. 1, 2008, pp. 142–158.

[24] Hicken, J. E., Zingg, D. W. "Induced-Drag Minimization of Nonplanar Geometries Based on the Euler Equations," AIAA Journal, Vol. 48, No. 11, 2010, pp. 2564–2575.